Controls on the explosivity of scoria cone eruptions: Magma segregation at conduit junctions

Pioli, Laura; Azzopardi, B. J.; Cashman, K. V.

How to cite

PIOLI, Laura, AZZOPARDI, B. J., CASHMAN, K. V. Controls on the explosivity of scoria cone eruptions: Magma segregation at conduit junctions. In: Journal of volcanology and geothermal research, 2009, vol. 186, p. 407–415. doi: 10.1016/j.jvolgeores.2009.07.014

This publication URL: https://archive-ouverte.unige.ch/unige:3382
Publication DOI: 10.1016/j.jvolgeores.2009.07.014

CONTROLS ON THE EXPLOSIVITY OF SCORIA CONE ERUPTIONS: MAGMA SEGREGATION AT CONDUIT JUNCTIONS

L. Pioli[1], B.J. Azzopardi[2], K. V. Cashman[3]

[1] Section des Sciences de la Terre, Université de Genève, Switzerland
[2] Department of Chemical and Environmental Engineering, University of Nottingham, UK
[3]Department of Geological Sciences, University of Oregon, USA

Abstract

Violent strombolian (transitional) eruptions are common in mafic arc settings and are characterized by simultaneous explosive activity from scoria cone vents and lava effusion from lateral vents. This dual activity requires magma from the feeder conduit to split into vertical and lateral branches somewhere near the base of the scoria cone. Additionally, if the flow is separated, gas and liquid (+ crystals) components of the magma may be partitioned unevenly between the two branches. Because flow separation requires bubbles to move independently of the liquid over time scales of magma ascent separation is promoted by low magma viscosities and by high magma H_2O content (i.e. sufficiently deep bubble nucleation to allow organization of the gas and liquid phases during magma ascent). Numerical modeling shows that magma and gas distribution between vertical and horizontal branches of a T-junction is controlled by the mass flow rate and the geometry of the system, as well as by magma viscosity. Specifically, we find that mass eruption rates (MER) between 10^3 and 10^5 kg/s allow the gas phase to concentrate within the central conduit, significantly increasing explosivity of the eruption. Lower MERs produce either strombolian or effusive eruption styles, while MER > 10^5 kg/s prohibit both gas segregation and lateral magma transport, creating explosive eruptions that are

not accompanied by effusive activity. These bracketing MER constraints on eruptive transitions are consistent with field observations from recent eruptions of hydrous mafic magmas.

Keywords: Basaltic volcanism; violent strombolian eruption; gas segregation

1. Introduction

Scoria cone eruptions are a common and spectacular form of mafic volcanic activity that often includes either simultaneous or alternating explosions and lava effusion. Scoria cones are common in subduction zones (Michoacan-Guanajato volcanic field, Mexico; Central Cascade, USA, Auckland volcanic field, New Zealand), continental rift zones (San Francisco volcanic field, USA; Pinacate volcanic field, Mexico) and at some central volcanoes (e.g., Etna and Vesuvius, Italy; Kīlauea, Mauna Loa, Mauna Kea, USA). Although most scoria cone eruptions are monogenetic (that is, single eruptive episodes), reoccupation of vents may also occur (e.g., Etna summit craters: Behnke et al, 2006; Cerro Negro: McKnight and Williams, 1997). Historical cone-forming eruptions have had durations of days to years, with time-averaged mass eruption rates (MERs) of 10^2 to ~10^5 kg/s. Lava flows are typically an important component of these eruptions and can constitute a minor or major fraction of the erupted mass (e.g. 94% by weight of the magma erupted during the 1971 eruption of Etna was emitted as lava; 39% by weight of lava in the Parícutin 1943-1952 eruption; Booth and Walker, 1973, Walker 1973a, Pioli et al. 2008).

Scoria cones are constructional features that change in form through time. Early-formed cones are commonly horseshoe-shaped, constructed around the active vent and

49 associated lava flow. This form permits lava effusion and explosions to occur from the
50 same vent(s). Protracted activity completes the cone by accumulation of scoria around
51 the vent, such that explosive eruptions become localized at the cone vent while lava flows
52 emerge from lateral vents located at the base of the cone. Gas emissions also localize at
53 the cone vent, as explosive eruptions emit substantial amounts of gas as a free phase and
54 scoria produced by explosive eruptions is typically more vesicular than co-erupted lava.
55 Thus a dual-vent configuration requires both volatile segregation (to power explosive
56 activity) and magma segregation into both vertical and lateral conduits (Krauskopf, 1948;
57 Behnke and Neri, 2003). Finally, volatile segregation requires sufficient transit time in
58 the conduit for bubble migration; from this perspective, we expect much more extensive
59 segregation for volatile-rich magmas (where gas exsolution may start at > 4-5 km below
60 the vent; Pioli et al., 2008) than in volatile-poor magmas, where most gas exsolution is
61 very shallow (Mangan and Cashman, 1996; Edmonds and Gerlach, 2007).
62 Pioli et al. (2008) suggested that the synchroneity of explosive and effusive activity is
63 a key characteristic of activity that has been termed "violent strombolian" (MacDonald,
64 1972) and is characterized by average mass fluxes of water-rich basalts that are
65 intermediate between strombolian and subplinian regimes. Violent strombolian
66 explosions are typically discontinuous and strongly pulsatory rather than steady (up to
67 120 explosions per minute have been described in 1943 Parictuin eruption by Foshag and
68 González-Reina, 1956). Related effusive activity may also be discontinuous and may or
69 may not exhibit a systematic relationship to explosive activity (Krauskopf, 1948).
70 Violent strombolian explosions produce pyroclasts that form composite deposits that
71 include a scoria cone, a tephra blanket, and lava flows spreading from lateral vents (e.g.,

72 Valentine et al., 2005; Pioli et al., 2008). This 'mixed' eruption style is unique to low
73 viscosity magmas and is generally associated with high initial water contents (i.e. arc
74 basalts, Wallace, 2005). Here we address the primary controls on mafic eruptive styles
75 by examining the physical conditions required for this dual activity, including the
76 structure of the feeding system and the contribution of volatile segregation to explosivity.
77

78 ## 2. Observational constraints on violent strombolian activity

79 The geometry of magma delivery systems beneath scoria cones is best observed in
80 older eroded monogenetic volcanoes, which reveal the syn-eruptive interplay between
81 dike intrusion, pyroclast sedimentation, and lava accumulation in the development of the
82 shallow magmatic conduit (Keating et al., 2008; Valentine and Keating, 2007). Feeder
83 systems are dikes with widths of 4-12 m at depths > 100 m. Exposed shallow conduits are
84 often complex, with multiple dikes and sills that provide evidence for extensive shallow
85 magma storage (e.g., Johnson et al., 2008). However, field studies of eroded cones
86 provide only crude constraints on the geometry of feeder systems during any individual
87 eruptive phase, as the preserved structure is the integrated result of the sequence of events
88 that comprise the volcano's history (Keating et al. 2008).

89 The dynamics of violent strombolian eruptions are best revealed by observations
90 of recent activity. Differentiation between central and lateral vents can occur within a few
91 hours (Etna 2001 and 2002 eruptions; Behncke and Neri, 2003; Andronico et al., 2005) or
92 may require weeks from the eruption onset (Parìcutin 1943-1952; Gonzàlez-Reyna and
93 Foshag, 1946). The latter example is particularly pertinent as it is the type example of a
94 violent strombolian eruption (e.g., Macdonald, 1972) and detailed reports provide

95 important constraints on the development and evolution of the lateral dike system and
96 related changes in eruption dynamics (summarized in Luhr and Simkin, 1993).

97 The Parícutin eruption started with the opening of a 50 m long fracture (Gonzàlez
98 -Reyna and Foshag, 1946). Within a few hours, mild explosive activity had focused in
99 the northern portion of the fracture and by the end of 24 hours, the resulting scoria cone
100 was about 30 m high. Lava emission started on the second day from the same crater
101 where the explosions were occurring, producing a horseshoe-shaped cone and a lava flow
102 (Gonzalez-Reyna and Foshag, 1946). Progressive scoria accumulation around the vent
103 gradually formed a complete cone, although it was initially subject to sector collapses
104 related to lava effusion. The cone acquired full stability in about one month, when it was
105 about 150 m high.

106 Cone stabilization coincided with the onset of the 'cineritic phase' of eruptive
107 activity, that is, violent strombolian explosions that formed ash-rich columns reaching
108 elevations of ≤ 6 km (Ordoñez, 1945) and contemporaneous emission of lava from lateral
109 vents at the base of the cone (Fig. 2). This activity continued for several months and
110 deposited an extensive tephra blanket composed of vesicular scoria (> ~ 60% vesicles;
111 Pioli et al., 2008). At the same time, dense (vesicularity < 30%; Wilcox, 1954) lava was
112 fed from vents located at the cone base or within the cone slope (Foshag and González-
113 Reyna, 1956; Fries, 1953). Observations at the crater suggested a vent diameter of 3-8 m.
114 Evidence of intrusion of lava within the cone during this time period is provided by
115 pronounced bulges observed on the cone slopes before the opening of a new boca or
116 reoccupation of an older vent. The only interruption of this pattern of activity came in late
117 1943, when a new vent formed about 1 km N of the volcano and caused the temporary

(2.5 months) shut off of the main cone. A new horseshoe-shaped scoria cone (the 'Zapichu' vent) caused the activity at the new vent to revert to mild explosions (hawaiian and strombolian) and lava effusion.

Parícutin was active for nine years (1943-1952), during which time the mass eruption rate (MER) declined (Fig. 1) while the dominant eruptive style changed from explosive (total MER $\geq 10^4$ kg/s) to mainly effusive (total MER $<10^4$ kg/s) activity. The composition of the erupted magma also changed in the latter part of the eruption (after 1946); this compositional variation appeared at the same time in both lava and tephra products (Wilcox, 1954; McBirney, 1987; Luhr, 2001; Pioli et al., 2008; Erlund et al., in revision), demonstrating a common (shallow) source for both types of activity.

Taken together, observations of activity at Parícutin suggest that (a) the separation between the vertical conduit and lateral lava channel system occurred at a shallow depth (within or at the base of the cone), (b) the cone structure modulated the opening of new lava vents, (c) gas preferentially accumulated in the vertical conduit (giving rise to explosive activity from the central vent), (d) the mass eruption rate (MER) controlled the proportion of magma emitted by explosive vs. effusive activity, and (e) the initial formation of lateral vents increased the explosivity of eruptions occurring at the cone.

3. **Numerical modeling**

As outlined above, there appears to be a relationship between the development of separate vertical and lateral conduits and the onset of violent strombolian activity. To explore this relationship, we consider the geometric configuration of a T-junction with a vertical, cylindrical pipe (the central conduit) and a lateral, horizontal cylindrical branch

141 (the lava channel; Fig. 2). A similar geometry was used by Menand and Phillips
142 (2007a,b) in their experimental investigation of gas segregation and accumulation in sills,
143 but our geometry differs in allowing flow out the lateral branch.

144 Two-phase flow splitting through a T-junction has been studied extensively in
145 engineering fields for water-air flows (e.g., Zetzmann, 1984; Mudde et al., 1993;
146 Azzopardi, 1999; Conte and Azzopardi, 1999; Wang et al. 2002, Azzopardi, 2006; Yang
147 and Azzopardi, 2007). In all cases, the distribution of liquid and gas phases is uneven
148 when gas and liquid are characterized by different velocities, i.e. the flow is separated.
149 This condition is satisfied for low viscosity, mafic magmas in many natural settings (e.g.,
150 Vergnoille and Jaupart, 1989; Wilson and Head, 1981). To a first approximation, the
151 phase distribution is controlled by the relative momentum fluxes of the two phases, with
152 the higher momentum phase concentrating in the vertical conduit. However, the mass
153 flow distribution also depends on the geometry of the junction, the pressure drops along
154 the two outlet conduits, and therefore the flow rates in them. These experiments also
155 demonstrate that the most important parameters defining the flow segregation at a T-
156 junction are conduit diameter, gas and liquid flux, and the ratio between gas and liquid
157 volumes downstream and upstream of the junction. Experiments characterized by high
158 liquid superficial velocities (that is, volumetric flow rate divided by the cross sectional
159 area of the conduit) at the entry of the junction (Zetzmann, 1984) distribute gas
160 preferentially into the lateral conduit. In contrast, experiments using lower inlet liquid
161 flow rates preferentially distribute gas into the vertical branch (Conte, 2000).

162 To apply this work to volcanic activity, we use the geometry shown in the inset of
163 Figure 2. We assume that the gas is steam with a density defined by the local pressure

and temperature, and that gas exsolution from the magma is negligible above the junction, although gas is allowed to expand to accommodate pressure changes. We vary magma viscosity, pressure, and channel diameter but set both outlets to atmospheric pressure. Pressure increases inwards along the pipes to reach the same value at the junction. Flows in the vertical and lateral outlets are adjusted until the pressures in the two conduit branches are the same at the junction.

3.1. Governing equations

The total pressure gradient along any of the branches is the sum of the effect of gravitational forces (G), friction loss (F) and acceleration of the fluid (A)

$$-\frac{dp_j}{dz_j} = -\frac{dp_{Gj}}{dz_j} - \frac{dp_{Fj}}{dz_j} - \frac{dp_{Aj}}{dz_j} \quad , \qquad (1)$$

where j refers to any of the three branches (1, 2, or 3). The pressure p_2 in the vertical branch is controlled by both the gravitational and frictional components whilst the pressure p_3 in the horizontal channel is controlled only by friction. Gas expansion effects due to depressurization were calculated in the pipes upstream the junction assuming equilibrium with local pressure. As it has been assumed that there is no change in the amount of exsolved gas, the acceleration component of pressure drop was taken to be negligible. Calculations confirmed that this was so except in the near neighbourhood of the outlets. The calculation approach is similar to that employed by Wilson and Head (1981) but allows the gas and liquid to have different velocities and the gas to affect the frictional component.

Pressure changes were determined by integrating the following equations:

186 $$p_2(z_2) = \int_0^{z_2} \left(\left(\varepsilon_g \ \rho_g \ + (1 \ - \ \varepsilon_g) \ \rho_l \right) g + \frac{4 \ f_{l2}}{D_2} \ \frac{\rho_l u_{ls2}^2}{2} \left[1 \ + \ \frac{C}{X} \ + \ \frac{1}{X^2} \right] \right) dz, \text{ and} \quad (2)$$

187 $$p_3(z_3) = \int_0^{z_3} \left(\frac{4 \, f_{l3}}{D_3} \ \frac{\rho_l u_{ls3}^2}{2} \left[1 + \frac{C}{X} + \frac{1}{X^2} \right] \right) dz, \quad (3)$$

188 with equation (2) representing pressure changes in the vertical branch (including both
189 gravitational and frictional forces) and equation (3) representing pressure changes in the
190 horizontal branch (which includes only the frictional force).

191

192 *3.2. Calculating the gravitational component*

193 The gravitational component includes the void fraction ε_g, which is calculated
194 using a drift flux approach to allow for different velocities of gas and liquid (Wallis,
195 1969):

196 $$\varepsilon_g = \frac{u_{gs}}{C_0 \, (u_{gs} + u_{ls}) + v_{gd}} \quad (4)$$

197 In these equations u_{ls} and u_{gs} are the surficial velocities of liquid and gas, respectively,
198 and they represent the velocities they would have if they were flowing alone in the
199 channel. v_{gd} is termed the gas drift velocity, that is the relative velocity of the gas phase,
200 and for bubble flows is given by:

201 $$v_{gd} = K_1 \left(\frac{\sigma \ g \ (\rho_l - \rho_g)}{\rho_l^2} \right)^{0.25}, \quad (5)$$

202 with K_1 = 1.53 (Harmathy, 1960), ρ is the phase density and σ is the liquid surface
203 tension.

204 The constant C_0 in equation (3) is called the *distribution factor* (Zuber and
205 Findlay, 1965) and compensates for the effects of velocity profiles in the gas and liquid

206 flows (that is, non-uniform distribution of gas in the flow); its value depends on whether
207 the flow of the gas and liquid is laminar or turbulent. Flow regime, in turn, is described
208 using the Reynolds (*Re*) number, a dimensionless parameter that relates inertial and
209 viscous forces:

210 $$Re = \frac{\rho_i u_{si} D_j}{\eta_i}, \qquad (6)$$

211 We calculate *Re* separately for the gas and liquid phases using appropriate values for
212 density (ρ), viscosity (η), and velocity (u). In cylindrical pipes, transition from laminar to
213 turbulent flow is expected at *Re* ~ 4000 (Coulson et al., 1996). In our simulations *Re* <
214 2000 for the liquid and *Re* > 2000 for the gas; we follow Zuber and Findlay (1965) in
215 using C_0=1.2 for this situation.
216
217 *3.3. Calculating friction*
218 The friction factor *f* in equations (2) and (3) is a dimensionless number that
219 represents the ratio between friction forces and forces normal to the pipe walls and is
220 calculated as $f = \frac{16}{Re}$ for *Re*<2000 and $f = \frac{0.079}{Re^{0.25}}$ for *Re*>2000. The frictional term
221 describes the frictional component of pressure drop along the vertical conduit (with
222 diameter D_2) and horizontal channel (with diameter D_3). The term in the square brackets
223 is a correction factor that incorporates the effect of the gas phase on the frictional
224 pressure drop (Azzopardi and Hills, 2003). It is based on the dimensionless Martinelli
225 parameter *X* (Lockhart and Martinelli, 1949), the square root of the ratio of frictional
226 pressure gradients for the liquid and gas, calculated from the mass flow rates, densities

227 and total channel cross sectional area:

228 $$X^2 = \frac{\left(\frac{dp_F}{dz}\right)_l}{\left(\frac{dp_F}{dz}\right)_g} \quad . \qquad (7)$$

229 The constant C in equations (2) and (3) is a correlating parameter depending on the
230 regime of each phase. It takes the value of 20 when both phases are turbulent, 5 if they
231 are both flowing in laminar regime, 10 when the liquid phase is turbulent and the gas
232 phase is laminar, 12 in the opposite condition (Chisholm, 1967).

233

234 *3.4. Conservation of mass*

235 Conservation of mass is satisfied when:

236 $$\dot{M}_{l1} = \dot{M}_{l2} + \dot{M}_{l3} \text{ and} \qquad (8)$$

237 $$\dot{M}_{g1} = \dot{M}_{g2} + \dot{M}_{g3}. \qquad (9)$$

238 The effect of redistribution of gas and liquid phases at the junction is given by an
239 empirical equation of Conte (2000), which fits experimental results of mass redistribution
240 in T junctions from Conte (2000) and Zetzmann (1984)

241 $$L' = \frac{\dot{M}_{l3}}{\dot{M}_{l1}} = \left(\frac{23.5}{\rho_l u_{l1}^2} + 0.5\right)\left(\frac{\dot{M}_{g3}}{\dot{M}_{g1}}\right), \qquad (10)$$

242 The liquid flow rate in the side branch, $\dot{M}_{l3}$ is chosen at the start of each simulation.
243 Equation (8) then gives the liquid flow rate in the vertical channel, $\dot{M}_{l2}$. The gas flow in
244 the side branch, $\dot{M}_{g3}$, is obtained from equation (9) and that in the vertical channel, $\dot{M}_{g2}$
245 using equation (10). The pressure drops in the two channels are then calculated using

246 equations (2) and (3) and $\dot{M}_{l3}$ is adjusted until the two pressure drops are equal.

247

248 *3.5. Model limitations and applicability*

249 The model conservation equations have general validity, however, calculation of the
250 gravitational pressure drop requires calculation of the drift velocity, which depends on
251 the flow regime. In this model calculations in equation (5) were made assuming a bubbly
252 flow regime. For slug flow it is usual to express the drift velocity in terms of the Froude
253 number *Fr* (White and Beardmore, 1962), the ratio between of inertial to buoyancy
254 forces:

255 $$Fr = \frac{u_i^2}{gD_j}. \qquad (11)$$

256 By substitution,

257 $$v_{gd} = Fr\sqrt{gD_j}. \qquad (12)$$

258 *Fr* is expected to vary between 0.1 and 0.345 (Seyfried and Freundt, 2000). However,
259 examination of the relative values of the terms in equation (4) shows that the first term in
260 the denominator is much larger that the second so the either equation (5) or (12) will give
261 very similar values of void fraction when inserted in equation (4). For this reason, even if
262 in our calculations we simulated bubbly flow regimes, the results can be extended with
263 good approximation to slug flows.

264

265 To ensure applicability and limitations of empirical parameters derived from
266 experiments on air-water systems, we compare the volcanic and experimental systems
267 using appropriate dimensionless parameters to define flow regimes. Relevant

dimensionless parameters for bubbly flows are Eotvös number *Eo*, that is the ratio between buoyancy and surface tension forces $Eo = \frac{\rho_l g D_j^2}{\sigma}$, Morton number *Mo*, relating viscous to surface forces $Mo = \frac{g\eta_l^4}{\rho_l \sigma^3}$, and Reynolds number *Re* (Grace, 1973; Kulkarni and Joshi, 2005). In basaltic magma flows, $Re_l < 10^3$, $10^5 < Eo < 10^7$, and $10^5 < Mo < 10^{10}$ (Seyfried and Freundt, 2000). *Fr* number is not expected to vary significantly respect within the range of simulation conditions (Seyfried and Freundt, 2000). For comparison, experiments of Zetzmann (1984) and Conte (2000) have $10^2 < Eo < 10^3$; $10^{-10} < Mo < 10^{-11}$, *and* $10^3 < Re_l < 10^5$. The differences between the natural and experimental conditions are thus large, which will affect both bubble shape and velocity. In particular, gas velocity in our simulations will be underestimated by about one order of magnitude because of the high *Mo* anticipated in volcanic systems (e.g., Rodrigue, 2004). This limitation will affect both pressure calculations and mass distributions, leading to an overestimation of the amount of gas that is directed into the lateral branch.

4. Results

4.1. Mass distribution

To model basaltic eruptions, we solve the equations for ρ_l=2800 kg/m^3, σ= 0.4 N/m calculate gas density at T=1442 K; we vary the vertical and lateral conduit diameters, vertical conduit length, gas and liquid mass fluxes, and liquid viscosity. In all the cases the length of the lateral conduit was taken to be √3 times the height of the vertical conduit above the junction, to reproduce the stable geometry of a scoria cone. Most calculations used a lateral branch diameter of 2 m, as solutions of the equation system were possible

290 for smaller diameters only at the lowest flow rates considered. This value is in agreement
291 with observed dikes and conduits at depths >100m (Keating et al., 2008).

292 In all of the simulations, the liquid and gas phases redistribute in the two branches
293 upstream of the junction. At low mass flux, the mixture is preferentially drained through
294 the horizontal branch until a saturation value, above which further mass flux increases are
295 accommodated in the vertical conduit (Fig. 3a). Mass distribution is controlled by the
296 relative diameter of the vertical and lateral branches and the height of the vertical branch
297 (which controls the pressure at the T-junction). As the diameter of the lateral branch
298 increases relative to that of the vertical branch, the vertical MER decreases and the lateral
299 MER increases (Fig. 3b). Increasing length of the vertical branch, (which simulates
300 increasing the height of the cone), increases the pressure at the junction diminishing the
301 effect of the diameter increase (Fig. 3b), although pressure is not very sensitive to small
302 variations of the side channel diameter (Fig. 3c).

303 Magma viscosity also affects partitioning of gas and liquid within the system. In
304 particular, increasing the magma viscosity dramatically decreases liquid drainage through
305 the lateral system, such that an order of magnitude increase in viscosity forces the
306 mixture to emerge vertically for a range of MER. This is not surprising, as the lateral
307 pressure drop is directly proportional to viscosity at low Reynolds numbers, as shown in
308 section 3.3. In contrast, the vertical pressure drop is more strongly controlled by the
309 gravitational component than frictional, thus the total pressure drop is not as sensitive to
310 an increase in viscosity.

311

312 4.2. *Phase distribution*

313 Gas distribution between the vertical and lateral branches is controlled by the total
314 MER, the geometry of the system, and the pressure at the junction. Gas is generally
315 partitioned into the vertical conduit except when the junction pressure is high and/or the
316 lateral channel diameter is large. Gas accumulates in the lateral branch when the gas
317 volume flux is low with respect to the magma volume flux. This condition can be
318 achieved either through lengthening the vertical branch (increasing junction pressure;
319 Fig. 4a) or by extensive pre-eruptive magma degassing. Under these conditions, the mass
320 of gas emerging with the lateral flow increases with the lateral conduit diameter (Fig. 4a),
321 The distribution of gas between the vertical and lateral branches, in turn, affects the
322 energetics of eruptions from the main vent, the lateral transfer of gas (via the magma)
323 through the cone, and the consequent vesicularity of the erupted lava.
324 The role of total MER in gas segregation is shown in Figures 4b and 4c. At low
325 MER, the percentage of gas emerging with the lateral flow increases with increasing total
326 MER and gas flux is larger in the lateral channel than the vertical conduit. In our
327 simulations, when flow rate exceeds 10^3 kg/s, pressure balance at the junction can be
328 achieved only if the diameter of the lateral branch is decreased (from 2 to 1.35 m at the
329 highest flow rates). Under these conditions, the gas flux in the lateral channel remains
330 constant and the percentage of gas in the lateral channel decreases as total flow rate
331 increases. The same result could be obtained with a larger diameter if significant wall
332 roughness were assumed.
333
334 **5. Discussion**
335 Modeling results indicate that flow splitting at a dike junction has the potential to

336 generate an unequal distribution of the bulk flow between the vertical and lateral conduits
337 as well as a redistribution of liquid and gas phases. Variable distribution of both the total
338 mass flux and the gas and liquid fluxes between the central and lateral vents can explain
339 both temporal variations in eruptive style and the simultaneous explosive and effusive
340 activity that is commonly observed during scoria cone eruptions. Our simulations suggest
341 that partitioning of magma between the vertical conduit and lateral channel is controlled
342 primarily by the total MER and geometry of the junction. Numerical modeling also
343 suggests that eruptions should be dominated by lateral vent activity when MER $<10^3$ kg/s,
344 above which the relative proportion of magma erupted from the central conduit increases
345 rapidly until the flow through the lateral conduit is completely suppressed at MER $>10^{5\text{-}6}$
346 kg/s (Fig. 5).

347 Modest variations in the diameter of the lateral channel affect not only the
348 redistribution of the magmatic mixture (Fig. 5) but can also change the segregation of gas
349 between the vertical and lateral branches, thus indicating that flow spitting between
350 central and lateral conduits has important implications for eruption dynamics. In general,
351 the higher momentum phase concentrates in the vertical branch and the lower momentum
352 phase in the lateral branch. Thus extensive phase segregation can occur only when the
353 flow is separated (i.e., gas bubbles are moving independently of the liquid), because this
354 is the only condition where the phases have different momentum. An additional effect of
355 gas segregation is enhancement of explosivity at the central vent.

356 Gas preferentially accumulates in the lateral branch only when the gas volume flux is
357 low with respect to the magma volume flux (i.e. the mixture has low vesicularity). This
358 condition can be achieved either by increasing the depth of the T–junction within the

359 cone or by pre-eruptive magma degassing. The former situation may serve to limit the
360 maximum height of scoria cones. Another factor that may affect gas accumulation in the
361 lateral branch is concentration of bubbles in the center of the flow (e.g., Lucas et al.,
362 2005), as magma is preferentially drained into the lateral branch from the side of the
363 conduit.

364 *5.1. Application of simulation results to activity at Parícutin*

365 Our primary goal was to explain the observed correlation between mass eruption
366 rate and the relative proportion of mass erupted from vertical (or lateral) vents (Fig. 1).
367 Our model results for variations in vertical and lateral eruption rates (Fig. 6) match
368 observed rates for Parícutin (Fig. 1) when the vertical and lateral conduit branches have
369 diameters of 5 and 2 m, respectively, and the cone height is 500 m. These parameter
370 values seem reasonable given the substantial cone height (300-400 m) and estimated vent
371 diameters (3-8 m in the cone; 1-3 m for the lateral bocas; Foshag and González-Reyna,
372 1956) observed during the cineritic phases of Parícutin's eruption. A magma viscosity of
373 300 Pa s is also reasonable given a bulk melt composition of 54-55 wt% SiO_2, H_2O
374 contents of ≤ 4 wt% (Pioli et al., 2008), and temperature of 1100˚C (Luhr, 2001).

375 While the results of our simulation do not uniquely constrain the geometry of
376 Parícutin's shallow feeder system, the sensitivity of the simulation to variations in both
377 lateral channel dimension and magma viscosity does not allow much latitude in these
378 parameters. Moreover, our simulations suggest that the lateral branch should saturate at
379 $10^3 < \text{MER} < 10^4$ kg/s given magma properties and channel geometries appropriate for
380 the 1943 eruptive activity at Parícutin; higher MER require partitioning into the vertical
381 branch.

382 A second goal was to test the hypothesis that the onset of cineritic activity at Parícutin
383 can be explained by development of a junction within (or just below) the cone that feeds
384 simultaneous eruptions from the scoria cone vent and effusive vents at the base of the
385 cone. By definition, there is no segregation of the flow when the cone is incomplete. Our
386 simulations show that at MERs appropriate for early phases of the Parícutin eruption,
387 completing the cone would have promoted extensive gas segregation into the vertical
388 branch.

389 Our results also allow us to speculate on the nature of the Zapichu episode (that is, the
390 time period when activity shifted to a lateral vent). Krauskopf (1948) suggested that the
391 lateral vent was connected to the main feeder conduit at a depth of 600-700 m below the
392 one. Our simulations would suggest that depth, which would have doubled the junction
393 pressure, which would have caused the gas to segregate strongly into the lateral dike.
394 This predictions corresponds with observations, as explosive activity at the central vent
395 ceased at this time, while pyroclasts emitted from the Zapichu vent were described as
396 unusually vesicular. Additionally, strombolian to Hawaiian activity at the new Zapichu
397 cone (limited gas segregation) is consistent with the horseshoe shape of the new vent
398 structure.

399 *5.2. A general mechanism?*

400 A compilation of historic basaltic eruptions shows that simultaneous tephra and lava
401 production occurs over a limited range of mass eruption rates (MER= 10^3-10^5 kg/s; Table
402 1). Here we have included only eruptions of water-rich (subduction zone) basalts, where
403 volatile segregation can commence within feeder conduits (e.g., Pioli et al., 2008). We
404 measure the relative importance of explosive activity (that is, gas-enriched magma that is

405 segregated into the vertical conduit) by determining the ratio between the mass of the
406 tephra blanket and the entire eruptive mass (e.g., tephra blanket, scoria cone, and lava
407 flows). As illustrated in Figure 7, the results show striking similarities with numerical
408 modeling results: eruptions with MER $<10^3$ kg/s do not form tephra blankets; between
409 10^3 and 10^5 kg/s there is a positive relationship between MER and blanket mass;
410 MER$\geq 10^5$ creates purely explosive eruptions (subplinian to Plinian).

411 The transitional (violent strombolian) regime is characterized by explosive activity
412 (with eruption columns to $\leq \sim 6$ km height) accompanied by lava effusion from the base
413 of the cone (e.g., Krauskopf, 1948). Additionally, eruptions within this regime show a
414 direct correlation between explosivity, as defined by tephra production, and magma flux
415 (Fig. 7). Our modeling shows that simultaneous eruption of tephra from the cone and
416 lava flows from lateral vents requires segregation of bubbly magma into a gas-rich
417 mixture that ascends through the central conduit and gas-poor lava flowing in the lateral
418 system. This gas segregation must occur at a shallow depth (within or just below the
419 scoria cone), as high junction pressures serve to force the flow into the horizontal, rather
420 than the vertical, branch (e.g., the Zapichu episode). Segregation is also limited to
421 volatile-rich low viscosity magmas, conditions that promote separated flow of the gas and
422 liquid phases. We therefore conclude that the dual activity that characterizes violent
423 strombolian activity is unique to mafic eruptions of sufficient duration to construct
424 complete scoria cones and with 10^3<MER<10^5 kg/s.

425 When magma flow exceeds 10^5 kg/s, gas segregation is no longer possible, flow into
426 the lateral conduit ceases, and we would expect eruptive activity to take the form of
427 sustained columns (subplinian to Plinian activity). This prediction is consistent with

428 estimated MER for a paroxysmal eruption of Stromboli in 2003 (MER > 10^5 kg/s; Rosi et
429 al., 2006), a subplinian eruption of Shishaldin volcano in 1999 (MER = 2.5×10^6 kg/s;
430 Stelling et al., 2002) and for Plinian eruptions of Mt. Etna in 122 BC (Coltelli et al.,
431 1998) and Tarawera 1886 (Houghton et al., 2004), which had MERs of $5\text{-}10 \times 10^7$ kg/s.

432 At eruption rates below 10^3 kg/s, degassing dominates, producing either lava effusion
433 and/or mild explosive activity. Observations at Stromboli suggest that magma fluxes > ~
434 400 kg/s produce lava flows, while MER < ~ 100 kg/s reflect an effectively static magma
435 column where magma is ejected by bubble bursting at the surface at a rate controlled by
436 the gas flux (e.g., Chadwick et al., 2008). Low MER will also promote progressive
437 closure of the lateral channel because of the decrease in channel diameters required to
438 achieve pressure balance, as described by Ripepe et al. (2005) for the 2002-2003 eruptive
439 crisis at Stromboli. However, complete conduit closure cannot be modeled with our
440 calculations because they do not take into account viscoelastic properties of the wall
441 rocks.

442 5.3. *The role of viscosity*

443 Our simulations also provide insight into the role that magma viscosity might play
444 in modulating eruption style. Increasing the viscosity of the magma liquid drainage
445 through the lateral system (Fig. 3c). Even a modest increase in viscosity (from 300 to
446 3000 Pa s) has a significant impact on flow splitting, a result that is consistent with the
447 increasing time scale required for gas phase separation in viscous fluids. Thus we would
448 expect that lateral flow of magma would be absent in eruptions of high viscosity magmas.
449 Observations of recent eruptive activity confirm this. In these systems, high MERs (>~
450 10^6 kg/s) produce subplinian to Plinian eruptions while low MERs (< ~ 10^4 kg/s) produce

451 viscous flows and domes (e.g., Scandone and Malone, 1985; Scandone et al. 2007).
452 However, transitional activity in silicic systems (that is, activity produced by 10^4 < MER
453 < 10^6) differs from that of mafic systems in that explosive and effusive activity occur
454 sequentially rather than simultaneously, often with Vulcanian explosions followed by
455 dome effusion (e.g. Druitt et al., 2002; Wright et al, 2006). In these systems, the gas
456 segregation required to power the explosive events accumulates between, rather than
457 during, eruptive episodes.
458
459 **6. Conclusions**
460 Taken together, our results and the field observations suggest that shallow gas
461 segregation is particularly important for transitional eruptions of water-rich arc basalts,
462 which are characterized by high gas fluxes and separated flow conditions. In particular,
463 Figure 7 illustrates a dramatic increase in explosivity as MER changes from 10^3 to 10^5
464 kg/s, as documented by both the formation of convective columns capable of depositing
465 tephra blankets and by an increasing proportion of tephra with increased MER. For these
466 eruptions, explosivity can be strongly increased by shallow segregation of gas into
467 vertical conduits within early-formed scoria cones. This configuration, which is
468 associated with high gas fluxes and relatively low magma viscosity, causes efficient
469 redistribution of liquid and gas phases above (upstream of) the junction. Our simulations
470 predict that gas will concentrate increasingly in the vertical upper conduit as the total
471 MER exceeds ~ 10^4 kg/s, as shown in Fig. 4b, generating an abrupt increase of
472 explosivity with respect to 'normal' strombolian regimes. Numerical modeling indicates
473 that the segregation is more efficient for lower viscosity magmas, in agreement with

474 experimental results of Menand and Phillips (2007a,b).

475 Gas segregation is most efficient when the diameter of the lateral dike is small and
476 the magma flux is high. In contrast, gas will be preferentially concentrated in large
477 lateral conduits, particularly when junction pressures are high. Liquid is also segregated
478 into large lateral dikes, suggesting that widening of lateral dikes through time should both
479 increase the mass flux of lava from lateral vent and increase the lava vesicularity.
480 Increasing viscosity, which increases the pressure drop across the lateral conduit, also
481 enhances vertical magma flow. Together, temporal changes in scoria cone height (which
482 controls junction formation and pressure), mass eruption rate (which typically diminishes
483 with time) and magma viscosity (which changes with composition and crystallinity) can
484 explain observed changes in the eruption dynamics of violent strombolian eruptions.
485 More generally, we demonstrate that shallow gas segregation processes affect the
486 intensity and importance of both explosive and effusive components of mafic volcanism.

487 Our results cannot be extended to fissure eruptions, where spatial differentiation
488 of vents is likely related to the dynamics of magma rise within the dike and large MER
489 ($>10^3$kg/s, Keszthelyi et al., 2006) can be achieved without significant explosive
490 dynamics. They are also not appropriate for volatile-poor Hawaiian eruptions, where
491 vesiculation is sufficiently shallow that separated flow is unlikely except at very low
492 effusion rates (e.g., Mangan and Cashman, 1996; Gerlach and Edmonds, 2007). Finally,
493 this numerical model does not attempt to describe the fragmentation of magma that is
494 expected to occur at shallow depths within the scoria cone, as required by the eruptive
495 dynamics, the extensive tephra deposits, and the textural and petrographic characteristics
496 of the Paricutin tephra (Erlund et al., 2009).

ACKNOWLEDGMENTS

L.P was supported by NSF EAR0510493 (to KVC) and Swiss National Science Foundation FNSFN 200021-122268 projects. The authors wish to thank M. Ripepe and M. James for careful reviews and L. Wilson for editorial handling of the manuscript. We would also like to acknowledge our debt to Jim Luhr, who provided us with strong support for this project, and to both Jim Luhr and Tom Simkin for their wonderful book on Parícutin. We will miss them both.

APPENDIX

List of symbols

D = diameter

f = friction factor

g= gravitational acceleration

p= pressure

u= velocity

u_s = superficial velocity

v_{gd} = gas drift velocity

z = vertical length

σ= liquid surface tension

ε_g = void fraction

η= viscosity

ρ= density

Eo= Eotvos number

Fr= Froude number

Mo= Morton number

Re= Reynolds number

List of subscripts

1, 2, 3 refer to branches 1, 2, 3 of the junction, as numbered in fig. 2

l, g refer to liquid and gas, respectively

i refers to any of the phases considered (liquid or gas)

528 j refers to any of the branches of the junction (1,2,3)

529

529 **References**

530 Andronico, D., Branca, S., Calvari, S., Burton, M., Caltabiano, T., Corsaro, R.A., Del
531 Carlo, P., Garfi, G., Lodato, L., Miraglia, L., Muré, F., Neri, M., Pecora, E., Pompilio,
532 M., Salerno, G., Spampinato, L., 2005. A Multidisciplinary study of the 2002-2003 Etna
533 eruption: insights into a complex plumbing system. Bull. Volcanol. 67: 314-330.
534 Arrighi, S., Principe, C., Rosi, M., 1999. Violent Strombolian and Subplinian eruptions at
535 Vesuvius during post-1631 activity. Bull. Volcanol. 63: 126-150.
536 Azzopardi, B.J., 1999. Phase split at T-junctions. Multiph. Sci. Techn. 11: 223-329.
537 Azzopardi. B.J., 2006. Gas Liquid flows. Begell House, Redding, CT, 331 p.
538 Azzopardi, B.J., Hills, J., 2003. One dimensional models for pressure drop, empirical
539 equations for void fraction and frictional pressure drop and pressure drop and other
540 effects in fittings. In: W. Bertola (Editor), Modeling and experimentation in two-phase
541 flow, Springer, Wien, pp. 157-220.
542 Behncke, B., Neri, M., 2003. The July-August 2001 eruption of Mt. Etna (Sicily). Bull.
543 Volcanol. 65*:* 461-476.
544 Behncke, B., Neri, M., Pecora, E., Zanon, V., 2006. The exceptional activity and growth
545 of the southeast crater, Mount Etna (Italy), between 1996 and 2001. Bull. Volcanol. 69:
546 149-173.
547 Bertagnini, A., Landi, P., Santacroce, R., Sbrana, A., 1991. The 1906 eruption of
548 Vesuvius: from magmatic to phreatomagmatic activity through the flashing of a shallow
549 depth hydrothermal system. Bull. Volcanol. 53: 517-532.
550 Booth, B., Walker, G.P.L., 1973. Ash deposits form the new explosion crater, Etna 1971.
551 Phil. Trans. R. Soc. London 274: 147-151.
552 Chisholm, D., 1967. A theorethical basis for the Lockhart-Martinelli correlation for two-
553 phase flow. Int. J. Heat Mass Transfer 10: 1767-1778.
554 Chadwick, W.W., Cashman K.V., Embley, R.W., Matsumoto, H., Dziak, R.P., de Ronde,
555 C.E.J., Lau, T.K., Deardoff, N., Merle, S.G., 2008. Direct video and hydrophone
556 observations of submarine explosive eruptions at NW Rota-1 volcano, Mariana arc. J.
557 Geophys. Res. 113: B08S10, doi:10.1029/2007JB005215.
558 Coltelli, M., Del Carlo, P., Vezzoli, L., 1998. Discovery of a Plinian basaltic eruption of

559 Roman age at Etna volcano, Italy. Geology 26: 1095-1098.
560 Coltelli, M., Del Carlo, P., Pompilio, M., Vezzoli, L., 2005. Explosive eruption of a
561 picrite: the 3930 BP subplinian eruption of Etna volcano (Italy). Geophys. Res. Lett. 32,
562 L23307, doi:10.1029/2005GL024271.
563 Conte, G., 2000. An experimental study for the characterisation of gas/liquid flow
564 splitting at T-junctions. Ph.D. thesis, University of Nottingham.
565 Conte, G., Azzopardi, B.J. 1999. The split of slug/churn flow at a vertical T-junction**.** 2nd
566 Int. Symp. on Two-phase Flow Modelling and Experimentation, Pisa, 23-26 May.
567 Coulson. J.M., Richardson, J.F., Backhurst, J.R., Harker, J.H., 1996. Chemical
568 Engineering. Vol. 1: Fluid flow, Heat transfer and Mass Transfer. Butterworth-
569 Heinemann, Oxford, 775 pp.
570 Druitt, T.H., Young, S.R., Baptie, B., Bonadonna, C., Calder, E.S., Clarke A.B., Cole,
571 P.D., Harford, C.L., Herd, R.A., Luckett, R., Ryan, G., Voight, B., 2002. Episodes of
572 cyclic vulcanian explosive activity with fountain collapse at Soufriere Hills volcano,
573 Montserrat. In: T.H. Druitt, B.P. Kokelaar (Editors), The eruption of Soufriere Hills
574 volcano, Montserrat, from 1995 to 1999. Geol. Soc. Memoir 21:281-306.
575 Edmonds, M., Gerlach, T.M., 2007, Vapor segregation and loss in basaltic melts.
576 Geology 35: 751-754.
577 Erlund. E.J., Cashman, K.V., Wallace, P.J., Pioli, L., Rosi, M., Johnson, E., Delgado
578 Granados, H., 2009, Compositional evolution of magma form Parícutin volcano, Mexico:
579 the tephra record. Submitted to J. Volc. Geotherm. Res.
580 Fedotov, S.A., Balesta, S.T., Dvigalo, V.N., Razina A.A., Flerov, G.B., and Chirkov
581 A.M., 1984. New Tolbachik volcanoes. In: S.A. Feodtov (Editor), The Great Tolbachik
582 fissure eruption, 1975-1976. Nauka, Moskov, Russia, pp. 275-279.
583 Foshag, W.F., González-Reina, J., 1956. Birth and development of Parícutin Volcano
584 Mexico. U.S. Geol. Surv. Bull. 965: 355–489.
585 Fries, C.J., 1953. Volumes and weights of pyroclastic material, lava, and water erupted
586 by Parícutin volcano, Michoacan, Mexico. Trans. Am. Geophys. Union 34: 603–616.
587 Grace, J.R., 1973. Shapes and velocities of bubbles rising in infinite liquids. Trans. Inst.
588 Chem. Eng. 514: 116-120.
589 Gonzàlez-Reina, J.Jr., Foshag, W., 1947. The birth of Parícutin. Smithsonian Inst Ann.

590 Rpt. 1946: 223-234.
591 Gurenko, A.A., Belousov, A.B., Trumbull, R.B., Sobolev, A.V., 2005. Explosive basaltic
592 volcanism of the Chikurachki volcano (Kurile arc, Russia): insights on pre-eruptive
593 magmatic conditions and volatle budget revealed from phenocryst-hosted melt inclusione
594 and groundmass glasses. J. Volcanol. Geotherm. Res. 147: 203-232.
595 Harmathy, T.Z., 1960. Velocity of large drops and bubbles in media of infinite or
596 restricted extent. AIChE J. 6: 281-288.
597 Hill, B.E., Connor ,C.B., Jarzemba, M.S., La Femina, P., Navarro, M., Strauch, W., 1998.
598 1995 eruption of Cerro Negro volcano, Nicaragua, and risk assessment for future
599 eruptions. Geol. Soc. Am. Bull. 110: 1231-1241.
600 Houghton, B.F., Wilson, C.J.N., Del Carlo, P., Coltelli, M., Sable, J.E., Carey, R., 2004.
601 The influence of conduit processes on changes in style of basaltic Plinian eruptions:
602 Tarawera 1886 and Etna 122 BC. J. Volcanol. Geotherm. Res. 137: 1-14.
603 Johnson, E.R:, Wallace, P.J., Cashman, K.V., Delgado Granados, H., Kent, A.J.R., 2008,
604 Magmatic volatile contents and degassing-induced crystallization at Volcan Jorullo,
605 Mexico: implications for melt evolution and the plumbing systems of monogenetic
606 volcanoes. Earth Planet. Sci. Lett. 269: 478-487.
607 Keating, G.N., Valentine G.A., Krier D. J., Perry F.V., 2008, Shallow plumbing systems
608 for small-volume basaltic volcanoes. Bull. Volcanol. 70: 105-113.
609 Keszthelyi, L., Self, S., Thordarson, T., 2006. Flood lavas on the Earth, Io and Mars. J.
610 Geol. Soc. 163: 253-264.
611 Kulkarni, A.A., Joshi, J.B., 2005. Bubble formation and bubble rise velocity in gas-liquid
612 systems: a review. Ind. Eng. Chem. Res. 44:5873-5931.
613 Krauskopf, K., 1948. Mechanism of eruption at Parícutin Volcano, Mexico. Bull. Geol.
614 Soc. Am. 59: 711–732.
615 Lockhart, R.W., Martinelli, R.C., 1949. Proposed correlation of data for isothermal two-
616 phase two-component flow in pipes. Chem. Eng. Prog. 45: 39-48.
617 Lucas, D., Krepper, E., Prasser, H.-M., 2005. Development of co-current air-water flow
618 in a vertical tube. Int. J. Multiph. Flow 31: 1304-1328.
619 Luhr, J.F., Simkin, T., 1993. Parícutin: the volcano born in a cornfield. Geoscience Press,
620 Tucson, 427 pp.

621 Luhr, J.F., 2001. Glass inclusions and melt volatile contents at Parícutin Volcano,
622 Mexico. Contrib. Mineral. Petrol. 142: 261–283.
623 Macdonald, G.A., 1972. Volcanoes. Prentice-Hall inc., Englewood Cliffs, New Jersey,
624 510 pp.
625 Mangan, M.T., Cashman K.V., 1996, The structure of basaltic scoria and reticulite and
626 inferences for vesiculation, foam formation, and fragmentation in lava fountains. J.
627 Volcanol. Geotherm. Res. 73: 1-18.
628 Mannen, K., 2006, Total grainsize distribution of a mafic subplinian tephra, TB-2, from
629 the 1986 Izu-Oshima eruption, Japan: an estimation based on a theoretical model of
630 tephra dispersal. J. Volcanol. Geotherm. Res. 155: 1-17.
631 McBirney, A.R., Taylor, H.P., Armstrong, R.L., 1987. Parícutin re-examined: a classic
632 example of crustal assimilation in a calc-alkaline magma. Contrib. Mineral. Petrol. 95: 4–
633 20.
634 McKnight, S.B., Williams, S.N., 1997. Old cinder cone or young composite volcano?
635 The nature of Cerro Negro, Nicaragua. Geology 25: 339-342.
636 Menand, T., Phillips J.C., 2007a. Gas segregation in dykes and sills. J. Volcanol.
637 Geother. Res. 143: 393-408.
638 Menand, T., Phillips, J.C., 2007b. A note on gas segregation in dykes and sills at high
639 volumetric gas fractions. .J. Volcanol. Geotherm. Res. 162: 185-188.
640 Mudde, R.F., Groen, J.S., Van Den Akker, H.E.A., 1993. Two-phase flow redistribution
641 phsenomena in a large T-junction. Int. J. Multiphase Flow 19: 563-573.
642 Ordoñez, E., 1945. El volcan Parícutin. Comision Compulsora y coordinadora de la
643 investigacion Cientifica, Mexico, 138 pp.
644 Pioli, L., Erlund, E., Jonhson, E., Cashman, K., Wallace, P., Rosi M., Delgado-Granados,
645 H., 2008. Explosive dynamics of violent strombolian eruptions: the eruption of Parícutin
646 volcano 1943-1952 (Mexico). Earth Planet. Sci. Lett. 271: 359-368.
647 Ripepe, M., Marchetti, E., Ulivieri, G., Harris, A., Dehn, J., Burton, M., Caltabiano, T.,
648 Salerno, G., 2005. Effusive to explosive transition during the 2003 eruption of Stromboli
649 volcano. Geology 33: 341-344.
650 Rodrigue, D., 2004. A general correlation for the rise velocity of single gas bubbles. Can.
651 J. Chem. Eng. 82: 382-386.

652 Rosi, M., Bertagnini, A., Harris, A,J,L., Pioli, L., Pistolesi, M. Ripepe, M., 2006. A case
653 history of paroxysmal explosion at Stromboli: timing and dynamics of the April 5, 2005,
654 2003 event. Earth Planet. Sci. Lett. 243: 594-606.
655 Segerstrom K., 1950, Erosion studies at Parícutin. U.S. Geol. Surv. Bull. 965-A: 52 p.
656 Seyfried, R., Freundt, A., 2000. Experiments on conduit flow and eruption behavior of
657 basaltic volcanic eruptions. J. Geophys. Res. 105: 23727-23740.
658 Scandone, R., Malone S.D., 1985. Magma supply, magma discharge and readjustement
659 of the feeding system of Mount St. Helens during 1980. J. Volcanol. Geotherm. Res. 23:
660 239-252.
661 Scandone, R., Cashman, K.V., Malone, S.D., 2007. Magma supply, magma ascent and
662 the style of volcanic eruptions. Earth Planet. Sci. Lett. 253: 513-529.
663 Stelling, P., Beget, J., Nye, C., Gardner, J., Devine, J.D., George, R.M.M., 2002. Geology
664 and petrology of ejecta of the 1999 eruption of Shishaldin volcano, Alaska. Bull.
665 Volcanol. 64: 548-561.
666 Valentine, G, Krier, D., Perry, F.V., Heiken, G. 2005. Scoria cone construction
667 mechanisms, Lathrop wells volcano, southern Nevada, USA. Geology 33: 629-632.
668 Valentine, G., Keating, G., 2007. Eruptive styles and inferences about plumbing systems
669 at Hidden Cone and Little Black Peak scoria cone volcanoes (Nevada, U.S.A.). Bull.
670 Volcanol. 70: 105–113.
671 Vergniolle, S., Jaupart, C., 1989. Separated two-phase flow and basaltic eruptions. J.
672 Geophys. Res. 91: 12842-12860.
673 Walker, G.P.L., 1973a. A brief account of the 1971 eruption of Mount Etna. Phil. Trans.
674 R. Soc. London 274: 177-179.
675 Walker, G.P.L., 1973b. Explosive volcanic eruptions — a new classification scheme.
676 Geol. Rund. 62: 431–446.
677 Wallis, G.B., 1969. One-dimensional two phase flow. McGraw-Hill, New York, 409 pp.
678 Wallace, P.J., 2005, Volatiles in subduction zone magmas: concentrations and fluxes
679 based on melt inclusion and volcanic gas data. J. Volcanol. Geotherm. Res. 140: 217-240.
680 Wang, S., Shoji, M., 2002, Fluctuation characteristics of two-phase flow splitting at a
681 vertical impacting T-junction. Int. J. Multiphase Flow 28: 2007-2016.
682 White, E.T., Beardmore, R.H., 1962. The velocity of rise of single cylindrical air bubbles

683 through liquids contained in vertical tubes. Chem. Eng. Sci. 17: 351-361.
684 Wilson, L., Head, J., 1981. Ascent an emplacement of basaltic magma on the Earth and
685 Moon. J. Geophys. Res. 86: 2971-3001.
686 Wilcox, R.E., 1954. Petrology of Paricutín Volcano Mexico. U.S. Geol. Surv. Bull. 965:
687 281–353.
688 Wright, H.M.N., Cashman, K.V., Rosi, M., CIoni, R., 2007. Breadcrust bombs as
689 indivcators of vulcanian eruption dynamics at Guagua Pichincha volcano, Ecuador. Bull.,
690 Volcanol. 69: 281-300.
691 Yang, L., Azzopardi, B.J., 2007. Phase split of liquid-liquid two-phase flow at a
692 horizontal T-junction. Int, J. Multiphase flow 33: 207-216.
693 Zetzmann, K., 1984. Phase separation of air-water flow in a vertical T-junction. Ger.
694 Chem. Eng. *7*: 305-312.
695 Zuber, N., Findlay, J.A., 1965. Average volumetric concentration in two-phase flow
696 systems. J. of Heat Transf. 87: 453-468.
697

Figure caption

Figure 1. a) Year average effusive MER vs. Explosive MER for the Parìcutin eruption. Explosive MER was calculated using year cone and tephra blanket erupted volumes, effusive MER calculated after year erupted lava volumes as calculated in Pioli et al. (2008).

Figure 2. Sketch of scoria cone and lava channel. Inset shows the simplified geometry assumed for numerical modeling.

Figure 3. a) Effect of vertical channel diameter (indicated by the numbers in the inset) in flow redistribution upstream the junction. D_1/D_2=2.5 - 3.5; inset shows diameters of vertical branch for the three simulations. b) Effect of side branch diameter and main channel height on vertical and lateral mass flow rates emerging from the two exits. Black lines refer to the main channel flow, red lines are for the side branch flow. Total flow rate = 4×10^4 kg/s. Vertical channel height: continuous line = 100 m; thick dashed line = 350 m; thin dashed line = 500 m. c) Effect of side branch diameter and main channel height on pressure calculated that the junction point. Total flow rate = 4×10^4 kg/s. Vertical channel height: continuous line = 100 m; thick dashed line = 350 m; thin dashed line = 500 m d) Relationship between vertical and lateral mass flow rate. Height of main channel = 500 m. D_2=5 m, D_3=1.5 m; η_i: continuous line= 300 Pa s; dashed line = 3000 Pa s.

Figure 4. a) Effect of lateral dike diameter and height of main channel on percentage of gas emerging from the side branch, calculated with respect total gas flux. Total flow rate = 4×10^4 kg/s b); b) Effect of total flow rate and height of main channel on percentage of gas emerging from the side branch respect with the total gas flux. Vertical channel height: continuous line = 100 m; thick dashed line= 350 m; thin dashed line= 500 m.

Figure 5. Relative proportion of mass flowing through the junction into the vertical conduit vs. total mass flux rate. η_i=300 Pa s Thin line: D_2= 4 m, thick line: D_2=7 m.

Figure 6. Effects of magma splitting at a conduit junction when D_2= 5m, D_3=1.5 m, η_i =300 Pa s, cone height =500 m, compared with year average mass eruption rates of lava and tephra at Parìcutin volcano, as shown in Fig. 1.

Figure 7. a) Average MER vs. mass fraction of tephra blanket relative to total mass of erupted material of explosive eruptions of water-rich basalts. Violent strombolian

728 eruptions (central area) are characterized by variable erupted tephra, and MER between
729 10^4 to 10^5 kg/s, whereas purely explosive, subplinian to plinian eruption (higher MER)
730 are characterized by very little or no lava emission. Smaller MER eruptions (strombolian
731 to effusive) do not form substantial tephra blanket and have lower MER. Data listed in
732 Table 1.
733
734 **Table caption**
735 Table 1. Characteristics and references of basaltic eruptions plotted in figure 7. Asterisks
736 indicate Mass Discharge Rate data obtained from deposit characteristics.
737

Table 1
Click here to download Table: Table1.pdf

Eruption	Duration (days)	Average MER(Kg/s)	Blanket/ tot mass	Ref.
Parícutin 1943	214	5.56E+04	0.81	Fries, 1953; Krauskopf and Wiliams, 1946; Pioli et al., 2008; Segerstrom, 1950
Parícutin 1944	366	2.59E+04	0.61	
Parícutin 1945	365	1.86E+04	0.58	
Parícutin 1946	365	1.33E+04	0.48	
Parícutin 1947	365	1.11E+04	0.43	
Parícutin 1948	366	7.04E+03	0.18	
Parícutin 1949	365	4.60E+03	0.21	
Parícutin 1950	365	3.76E+03	0.20	
Parícutin 1951	365	3.90E+0.3	0.17	
Cerro Negro 1995	13	1.16E+04	0.20	Hill et al., 1998
Cerro Negro 1992	3.6	9.19E+04	1.00	
Cerro Negro 1850	10	1.72E+04	0.05	
Cerro Negro 1923	49	1.59E+04	0.61	
Cerro Negro 1947	13	3.43E+04	0.74	
Cerro Negro 1950	26	1.62E+04	0.99	
Cerro Negro 1960	89	1.93E+03	0.09	
Cerro Negro 1968	48	7.15E+03	0.39	
Cerro Negro 1971	10.6	5.28E+04	1.00	
Etna 122 BC	-	6.75E+07*	1.00	Coltelli et al., 1998
Etna 3930 BP	-	4.49E+07*	1.00	Coltelli et al., 2005
Etna 1971	69	2.60E+04	0.03	Booth and Walker, 1973; Walker 1973b
Etna 2001	6	2.73E+04	0.46	Behnke and Neri, 2003
Etna 2002	77	1.80E+04	0.53	Andronico et al., 2005
Etna 1999	-	2.83E+03	0.00	Behnke et al., 2006
Etna 1996-98	-	5.20E+01	0.00	
Shishaldin 1999	0.2	1.40E+07	1.00	Stelling et al., 2002
Izu Oshima 1986	6	8.10E+04	0.52	Mannen, 2006
Tolbachik 1975	72	2.29E+05	0.60	Fedotov et al., 1984
Tarawera 1886	0.2	1.09 E+08	1.00	Houghton et al., 2004
Vesuvius 1906	133.5	1.73E+05	0.80	Arrighi et al. 1999; Bertagnini et al., 1991
Chikurachki 1986	19	8.53E+04	0.74	Gurenko et al., 2005

Figure 1
Click here to download high resolution image

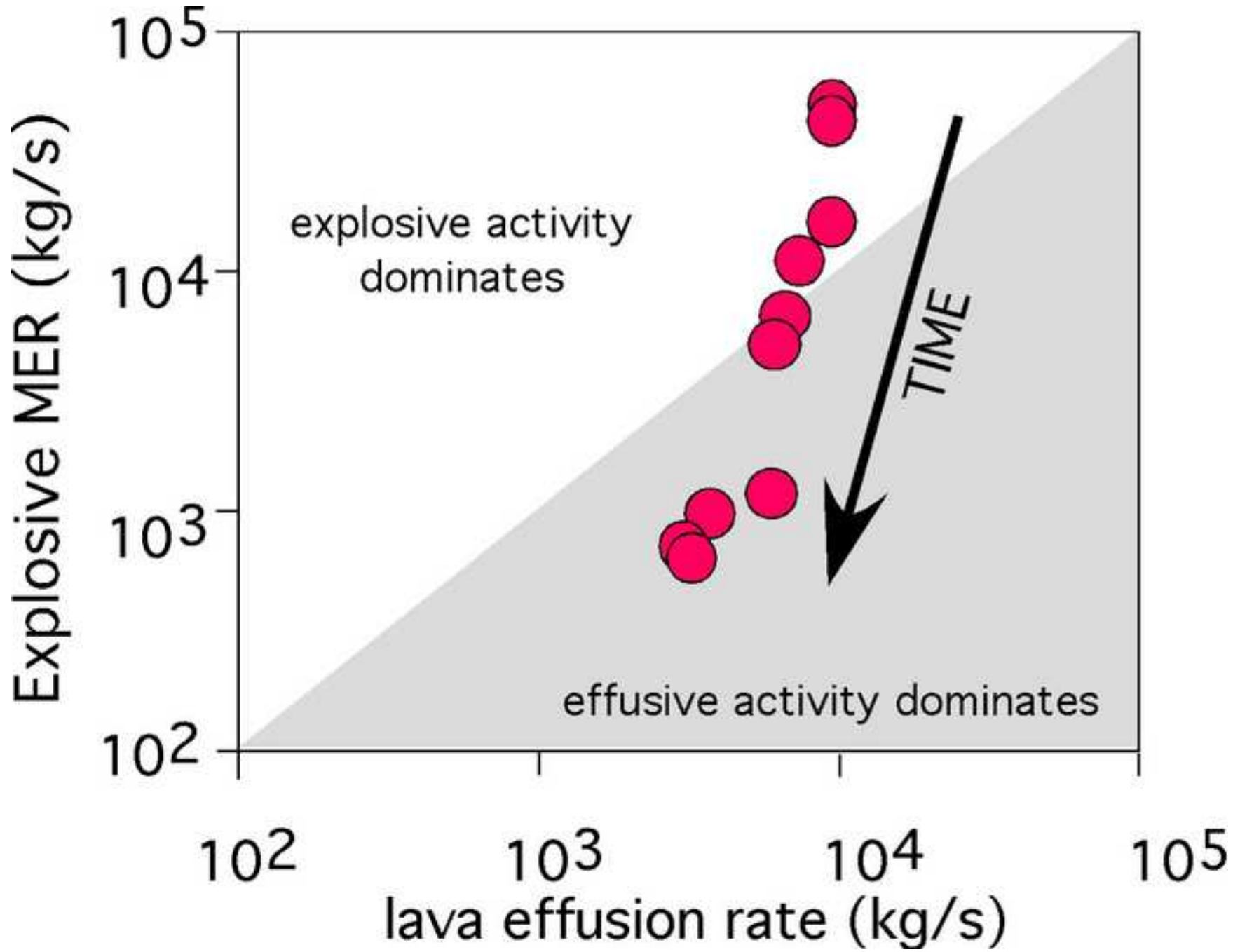

Figure 2
Click here to download high resolution image

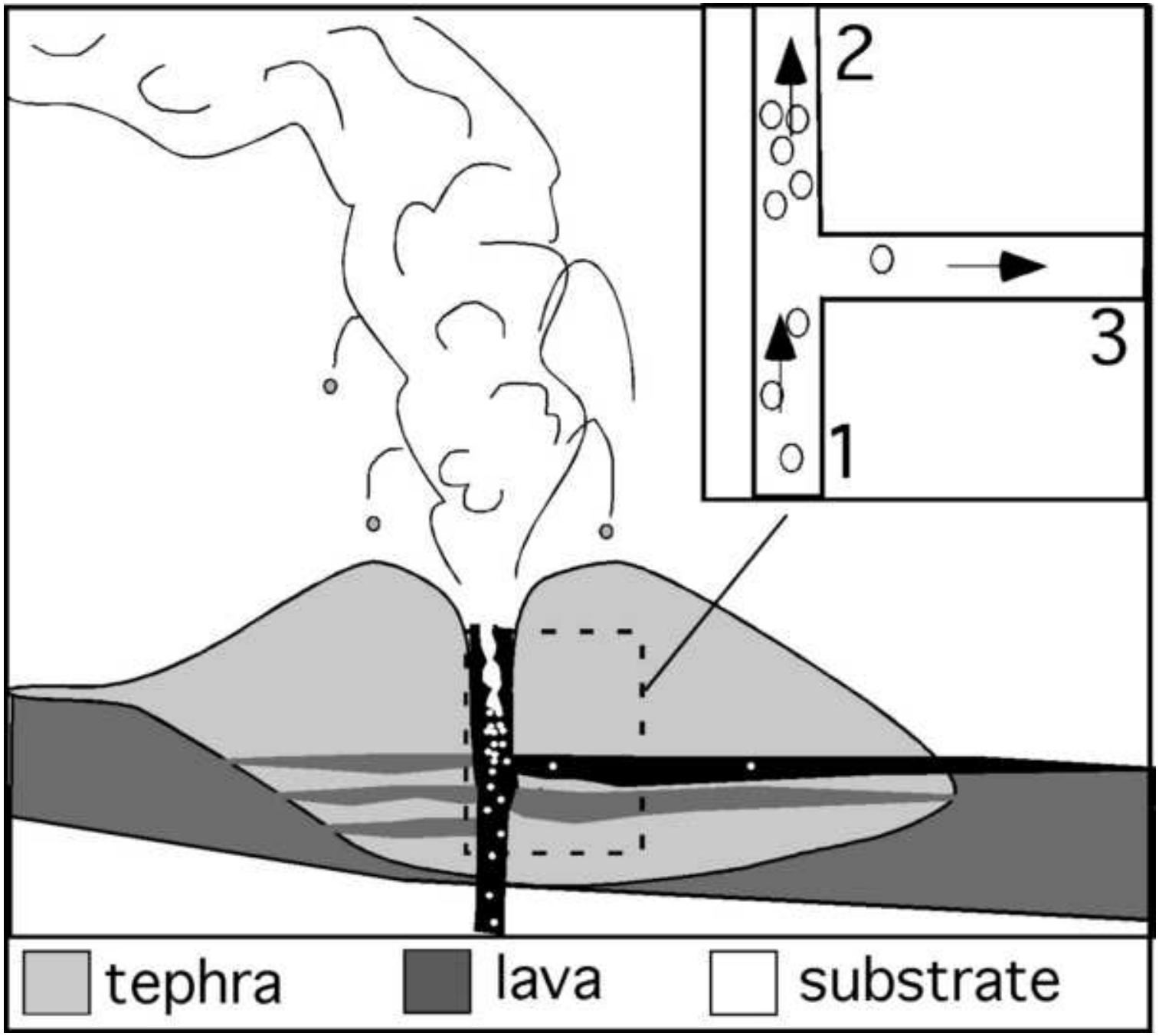

Figure 3
Click here to download high resolution image

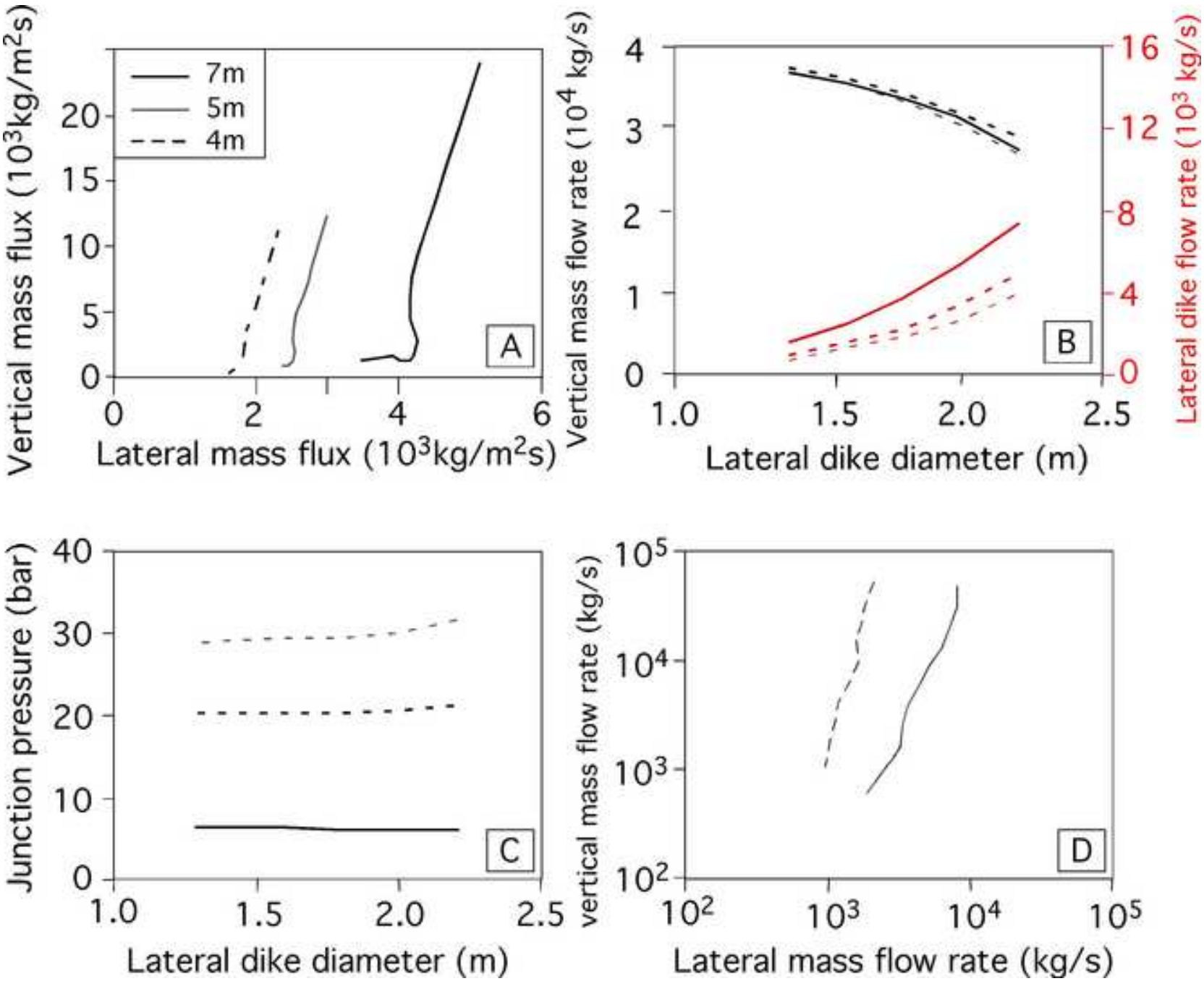

Figure 4
Click here to download high resolution image

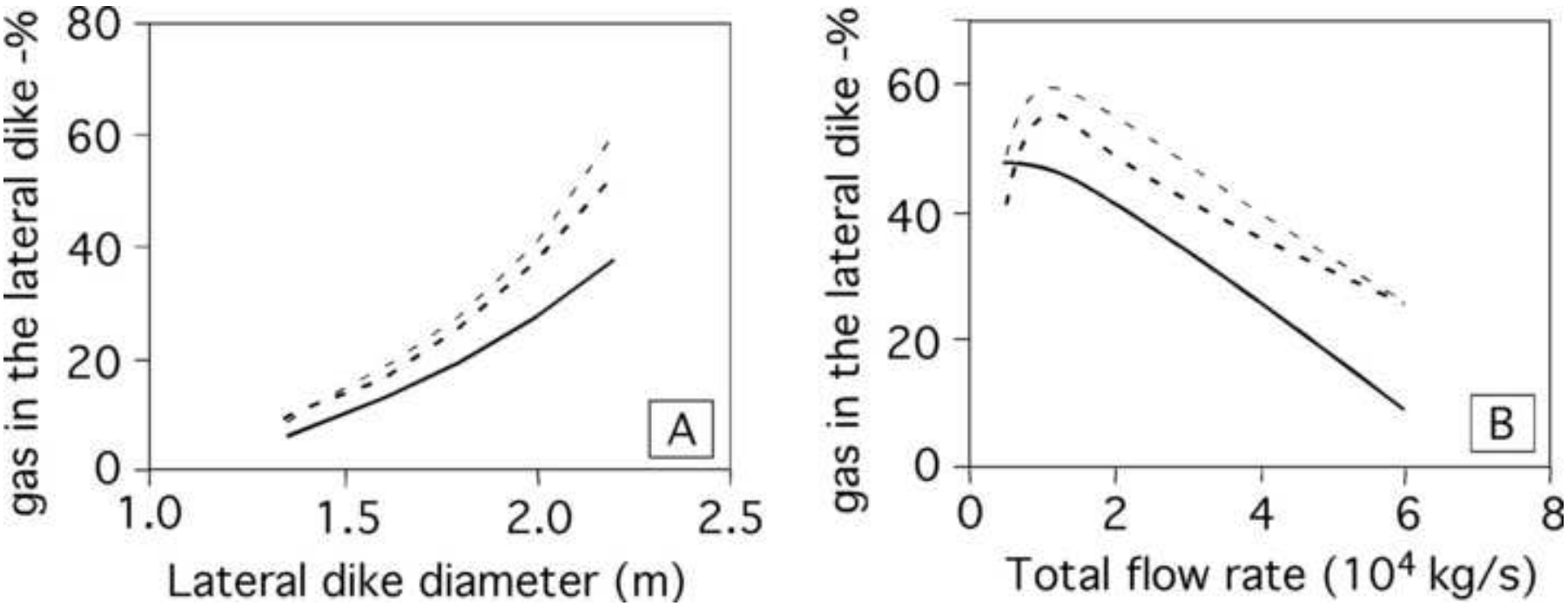

Figure 5
Click here to download high resolution image

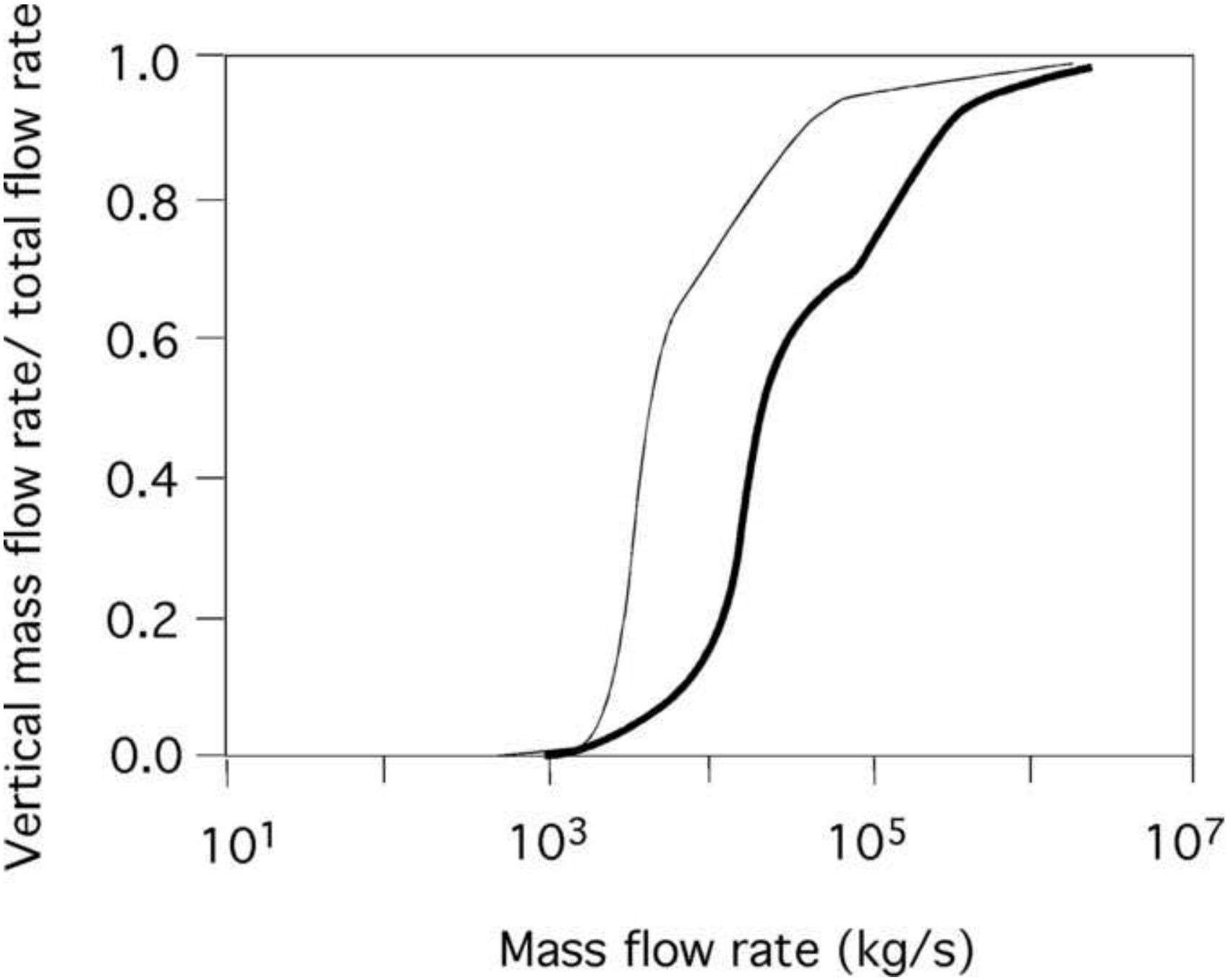

Figure 6
Click here to download high resolution image

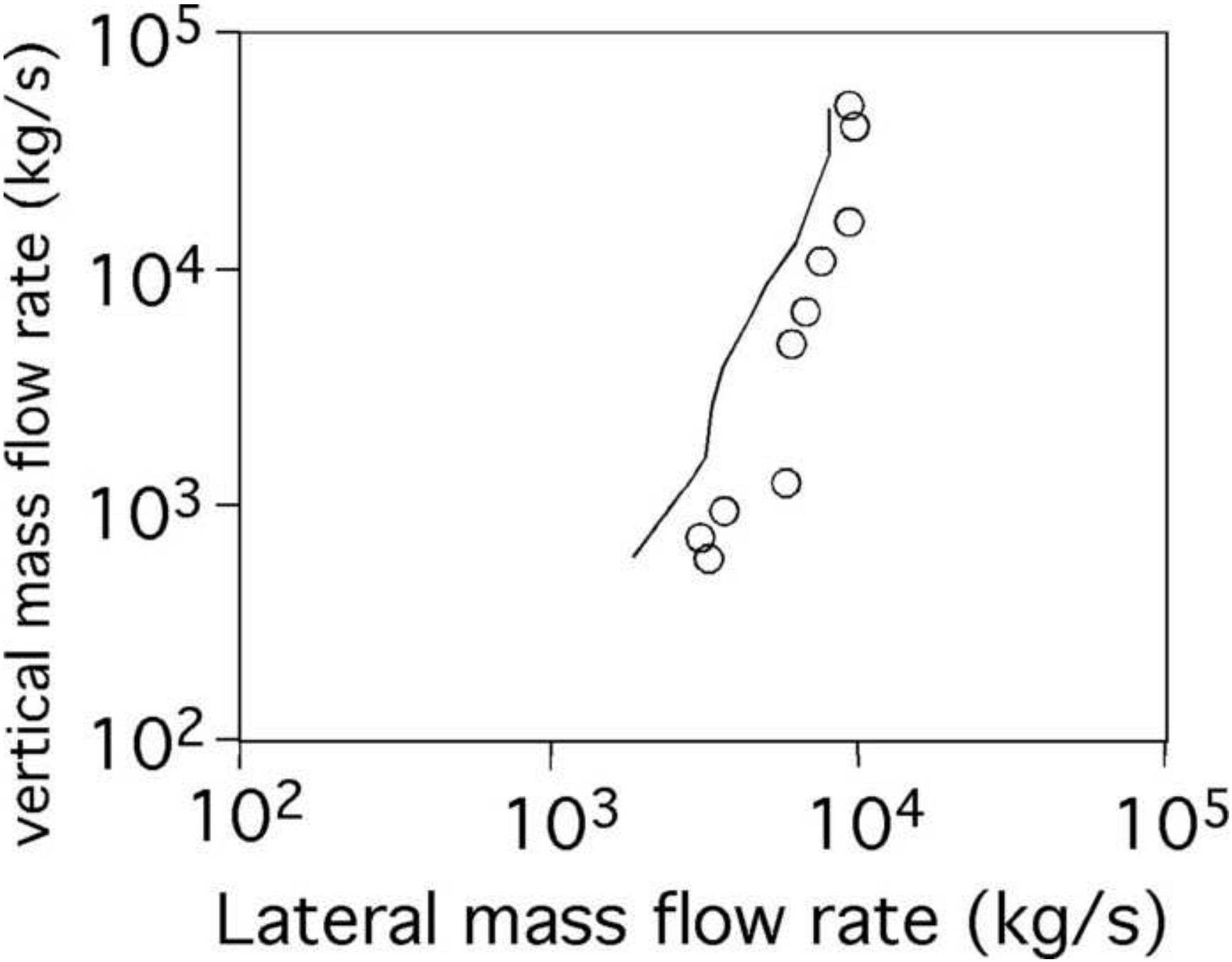

Figure 7
Click here to download high resolution image